Contents list available at IJRED website

International Journal of Renewable Energy Development

Journal homepage: https://ijred.undip.ac.id

Research Article

Investigation of wind veer characteristics on complex terrain using ground-based lidar

Undarmaa Tumenbayar [a] and Kyungnam Ko [b*]

[a] *Multidisciplinary Graduate School Program for Wind Energy, Jeju National University, 102 Jejudaehakro, Jeju, 63243, South Korea*

[b] *Department of Electrical and Energy Engineering, Jeju National University, 102 Jejudaehakro, Jeju, 63243, South Korea*

Abstract. The wind direction shift with height significantly influences wind turbine performance, particularly in relation to terrain conditions. In this work, wind conditions at 12 measurement heights ranging from 40 m to 200 m using a ground lidar, Windcube V2, installed on a 16 m tall building were analysed to examine the characteristics of wind veer angles in complex terrain. The measurement campaign was carried out from January 1st to December 31st, 2022, in the southeastern part of South Korea. The terrain complexity around the ground lidar system was evaluated using the ruggedness index (RIX), whose result was 14.06 percent corresponding to complex terrain. The ground lidar measurements were compared with mesoscale data, EMD-WRF South Korea, for the data accuracy check. Wind veer frequencies and wind roses were derived to identify directional shifts with height. Furthermore, diurnal, monthly, and seasonal variations of wind veer characteristics were analysed. Wind shear exponent factor (WSE) and turbulence kinetic energy (TKE) were calculated, and wind veer profiles were constructed based on these parameters. The relative errors of wind speeds were analysed for rotor equivalent wind speed (REWS) and hub height wind speed (HHWS), with REWS with wind veer correction, $REWS_{veer}$, as a reference. Additionally, atmospheric stability conditions were classified using WSE and TKE, and the vertical changes in wind veering were analysed according to the stability conditions. The findings reveal lower wind speeds exhibited larger wind veer values and fluctuations. The relative errors for the REWS and the HHWS were 0.04 % and 0.20 % on average, respectively. The study demonstrates that terrain conditions significantly impacted wind veer angles at heights below 100 m, whereas the influence diminished with increasing height above 100 m. The results could be helpful for wind farm developers to make decisions on the siting as well as the hub height of wind turbines on complex terrain.

Keywords: Wind data, Ground lidar, Complex terrain, Wind veer, Atmospheric stability

Received: 12th July 2023; Revised: 6th Oct 2023; Accepted: 26th Oct 2023; Available online: 5th Nov 2023

1. Introduction

Accurate prediction of wind conditions based on terrain characteristics is essential for efficient wind farm design and maximizing energy production. Mountainous areas with steep terrain pose challenges in estimating accurate wind conditions due to flow distortion caused by terrain complexity (Oh & Kim, 2015; Radünz *et al.*, 2020; Sharma *et al.*, 2021).

Traditionally, wind conditions such as wind speed and direction have been measured using met masts equipped with anemometers and wind vanes. However, installing met masts under remote and complex terrain conditions is often limited due to difficulties in transporting mast components and finding suitable flat areas for installation. Moreover, setting up a met mast taller than 100 m can be prohibitively expensive. To overcome these limitations, ground-based lidar technology has been widely adopted (Gottschall *et al.*, 2021; Nassif *et al.,* 2020). Lidar enables the capture of vertical wind profiles up to a height of 200 m, which is crucial for more accurate estimation of wind power production from modern large wind turbines (Leosphere, 2014). Extensive studies have been conducted to assess the measurement accuracy of ground-based lidar (Bodini *et al.*, 2019; Shin *et al.*, 2019), and high correlations between met masts and ground lidar measurements have been observed under various terrain conditions (Borraccino *et al.*, 2017; Yan *et al.*, 2022). Kim *et al.* (Kim *et al.*, 2016) found that ground lidar measurements exhibited an error of 2 % to 6 % in wind speeds under various terrain conditions.

Terrain conditions can significantly influence wind speed and direction changes with height, impacting the performance of large wind turbines. The change of wind speed with height is referred to as wind shear, while the change of wind direction with height is defined as wind veer. In order to estimate unknown wind speed at a point higher than a measurement height, wind power law and logarithmic law are often used in wind industry. However, there is no well-known equations for estimating wind veer at present.

Various studies on characteristics of wind shear has been widely performed over the decades (Gualtieri & Secci, 2011; Mason, 1992; Rehman & Al-Abbadi, 2005). Wind shear values are highly dependent on terrain conditions (Aghbalou *et al.*, 2018; Rasaq *et al.*, 2015), which influence power outputs of wind turbines. Wagner *et al.* (Wagner *et al.*, 2009, 2011) introduced the concept of wind shear correction using rotor equivalent wind speed (REWS), which was later added in the new publication of the International Electrotechnical Commission (IEC) 61400-12-1 2nd edition in 2017 (International Electrotechnical Commission, 2017). It was found that more accurate power outputs were derived from REWS taking into

* Corresponding author
Email: gnkor2@jejunu.ac.kr (K. Ko)

https://doi.org/10.14710/ijred.2023.56352
ISSN: 2252-4940/© 2024.The Author(s). Published by CBIORE

account the wind shear across the rotor diameter of a large wind turbine compared to those using the hub height wind speed (Barthelmie *et al.*, 2020; Shin *et al.*, 2019). Furthermore, in order to estimate much more accurate power outputs, the definition of the REWS, considering wind veer, is provided in Annex Q of IEC 61400-12-1 2nd edition. Taking the wind veer phenomenon into account is essential, particularly to estimate accurate power outputs as the rotor diameter of modern large wind turbines continues to increase. However, the REWS with wind veer correction, $REWS_{veer}$, is less likely to be considered due to its potentially minor effect on power outputs.

Wind veer is also a critical parameter in wind resource assessment (Durán et al., 2020; Shaw *et al.*, 2022), wind turbine wake (Abkar *et al.*, 2018; Englberger & Lundquist, 2020), fatigue load (Ennis *et al.*, 2018; Robertson *et al.*, 2019) as well as wind turbine power outputs (Lundquist, 2022; Sanchez Gomez & Lundquist, 2020a). Studies have indicated that clockwise wind veer leads to overperformance, while counterclockwise wind veer results in decreased turbine power outputs (Bardal *et al.*, 2015; Murphy *et al.*, 2020; Tumenbayar & Ko, 2023). The study of marine wind characteristics using lidar measurements revealed monthly and diurnal patterns of wind veers (Shu, Li, Chan, *et al.*, 2020). Gomez et al. (Sanchez Gomez & Lundquist, 2020b) analysed the diurnal pattern of wind veer and observed higher wind veer values during the morning transition period compared to the evening transition period. Shu *et al.* (Shu, Li, He, *et al.*, 2020) examined wind veer characteristics under various terrain conditions and found that wind veer values were comparatively higher in hilly terrain than in open-sea terrain. Additionally, Wharton *et al.* (Wharton et al., 2015) reported larger wind veer values in the lower part of the rotor swept area compared to the upper part. However, wind veer has received less attention compared to other factors such as wind speed, WSE, turbulence intensity (TI), and others.

The purpose of this work is to investigate the characteristics of wind veer on complex terrain using measurements from a ground based lidar. Wind veer angles are analysed in terms of diurnal, monthly, and seasonal variations, as well as in relation to wind shear exponent (WSE) and turbulence kinetic energy (TKE). The relative error was analysed for the REWS and hub height wind speed, HHWS, using $REWS_{veer}$ as the reference. Furthermore, vertical profiles of wind veer angles are examined under various atmospheric stability conditions.

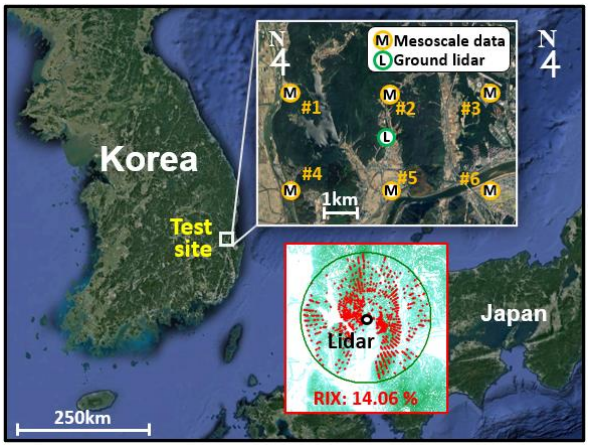

(a) Locations of test site, ground lidar and mesoscale data.

(b) Terrain conditions surrounding the lidar.

Fig. 1 Test site location and terrain condition surrounding the ground lidar.

2. Test setup and methodology

2.1 Test site and test instrument

Fig. 1 (a) shows the locations of the measurement site, the ground lidar and the six mesoscale reanalysis data points. The surrounding terrain conditions of the ground lidar instrument are presented in Fig. 1 (b). The measurement campaign was conducted in the southeastern part of South Korea. The ground lidar was installed on the rooftop of a 16 m tall building, situated at a latitude of 36°00'38.16" north and a longitude of 129°17'1.68" east. The six mesoscale data were utilized to check the accuracy of the ground lidar wind data.

The complexity of the terrain at the measurement site was assessed using the ruggedness index (RIX), which has been widely used over the decades in wind energy industries to classify the terrain complexity. In the RIX image, the red lines indicate terrain slopes steeper than the critical slope of 30 % within a radius of 3.5 km from the lidar. The RIX value is the ratio of the added length of the red lines to the sum of the lengths of the 72 radii from the lidar (Mortensen et al., 2008; Sletsjøe, 2020). In general, a site with the RIX value of 0 % is considered as a flat terrain, while a site with the 10 % or higher RIX value is considered as a complex terrain (Birkelund *et al.*, 2018). The measurement site in this work exhibited a RIX value of 14.06 %, indicating a complex terrain condition.

Table 1 presents the specifications of the ground lidar used in this study. The Windcube V2 ground lidar was used to measure 10-minute averaged wind conditions at 12 measurement points ranging from 40 m to 200 m in height. The wind measurements campaign conducted for one year, from January 1st to December 31st, 2022.

Table 1
Specification of test instrument

Ground lidar	Specification
Model	Windcube V2
Measurement range	40 ~ 200 m
Sampling rate	1 Hz
No. of measurement heights	12 heights
Analysed measurement points	40, 50, 70, 80, 90, 100, 110, 120, 130, 150, 180, 200 m

2.2 Data filtering

Wind measurements with an availability of less than 80 % or a carrier-to-noise ratio (CNR) of less than -23 dB were discarded following the guidelines provided in the ground lidar's user manual (Leosphere, 2014) and the study conducted by Kim *et al.* (Kim *et al.*, 2016). After the filtering, approximately 89.6 % of the data remained, which was used for the analysis in this study.

2.3 Methodology

First, the accuracy check was carried out between the ground lidar wind data and the reanalysis data of the EMD-WRF South Korea mesoscale data set near the lidar. The mesoscale data has a spatial resolution of 3x3 km with hourly temporal resolution (EMD International, n.d.). Then, the wind veer characteristics were analysed in terms of diurnal, monthly and seasonal variations as well as the WSE and TKE. The WSE and TKE were used for classifying the atmospheric stability conditions of the measurement site. Lastly, wind veer profiles were compared in accordance with stable, neutral and unstable conditions.

The wind veer angle per meter was analysed by the following equation (Gao *et al.*, 2021):

$$Wind\ veer = \frac{WD_U - WD_{1L}}{Z_U - Z_{1L}} \quad [deg./m] \qquad (1)$$

where, WD_U and WD_{1L} are the wind direction angles at the upper and the one lower level measurement heights, respectively. Z_U and Z_{1L} are the upper and the one lower level measurement heights, respectively. In general, a negative wind veer angle corresponds to backing wind, while a positive angle refers to veering wind. In this work, absolute values of wind veer were used for the analyses except wind veer frequency distribution of the section 3.3.

The dimensionless WSE, α, was evaluated by the following equation (Jung & Schindler, 2021):

$$\alpha = \frac{ln\,(V_U / V_{1L})}{ln\,(Z_U / Z_{1L})} \qquad (2)$$

where, V_U and V_{1L} are the wind speeds at the upper and the one lower level measurement heights, respectively.

The TKE at each measurement height was calculated by the following equation (St Martin *et al.*, 2016):

$$TKE = \frac{1}{2}\left(\overline{u'^2} + \overline{v'^2} + \overline{w'^2}\right) \quad [m^2/s^2\,] \qquad (3)$$

where, u', v', and w' are variances obtained from a 10-minute average of the latitudinal (u), longitudinal (v) and vertical (w) components of the wind at each measurement height, respectively.

When wind speed and wind direction across the turbine rotor diameter are constant, measurements at the hub height are representative for computing wind turbine power production. However, wind speed and wind direction at hub height are not always representative of the conditions at the turbine rotor, since those are susceptible to change depending on atmospheric stability as well as terrain complexity. Thus, not only the REWS, but also the wind speed considering the vertical profile of wind shear and wind veer across the rotor diameter, the $REWS_{veer}$, was analysed according to guidelines of the IEC 61400-12-1 3rd edition (International Electrotechnical Commission, 2022).

Fig. 2 presents the minimum measurement height requirements for the REWS and the $REWS_{veer}$ calculations. The

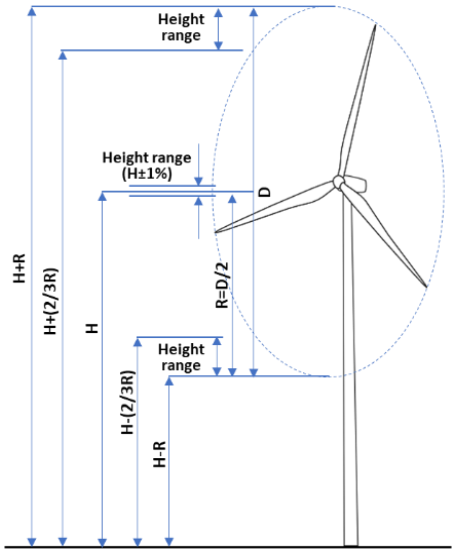

Fig. 2 REWS and $REWS_{veer}$ measurement scheme

minimum height requirements are between the hub height, H, minus rotor radius, R, and H minus 2/3 R for the lower height range, and between H plus R and H plus 2/3 R for the upper height range, while staying within ± 1 % of hub height. It is also recommended to have as many measurement heights as possible across the rotor swept area.

The REWS and the $REWS_{veer}$ are calculated by the following equations:

$$REWS = \left(\sum_{i=1}^{n_h} v_i^3 \frac{A_i}{A}\right)^{1/3} \quad [m/s] \qquad (4)$$

$$REWS_{veer} = \left(\sum_{i=1}^{n_h} (v_i cos\,(\varphi_i))^3 \frac{A_i}{A}\right)^{1/3} \quad [m/s] \qquad (5)$$

where, n_h is the number of measurement heights, and v_i is the wind speed measured at height i. φ_i is the angle difference between the wind direction at the hub height and section i. A and A_i are the swept area of the wind turbine rotor and the i^{th} section of the swept area, respectively.

In this work, a 2 MW reference wind turbine was used for the REWS and the $REWS_{veer}$ calculations, with a hub height and rotor diameter of 80 m and 87 m, respectively. The wind conditions at the heights of 40 m, 80 m and 124 m measured by the lidar system were used for the analysis. It was assumed that $REWS_{veer}$ is a reference in this work, since that takes both wind shear and wind veer into account.

The relative error for the wind speeds, WS, of HHWS and REWS was calculated by the following equation:

Table 2
Atmospheric stability regime according to WSE and TKE

Stability class	WSE	TKE [m^2/s^2]
Unstable condition	α < 0.11	TKE > 6.5
Neutral condition	0.11 < α < 0.17	3.0 < TKE < 6.5
Stable condition	α > 0.17	TKE < 3.0

$$Relative\ error = \left|\frac{WS - REWS_{veer}}{REWS_{veer}}\right| \times 100\ [\%]\ (6)$$

Lastly, the atmospheric stability regimes according to WSE and TKE are presented in Table 2 (St Martin et al., 2016). The atmospheric stability conditions at the measurement site were classified as unstable, neutral and stable. These conditions were analysed in relation to the wind veer characteristics in this study.

3. Result and discussion

3.1 Data accuracy check

In our previous works (Kang *et al.,* 2017; Kim *et al.,* 2016; Shin *et al.*, 2019; Tumenbayar & Ko, 2023), the same Windcube V2 as this work was used and it was observed that the coefficient of determination, R^2, between met masts and the ground lidar wind speeds were ranged from 0.96 to 0.99. This indicates high accuracy of the lidar measurements.

The hourly mesoscale data shown in Fig. 1 (a) during the same period as the lidar measurements were collected from every coordinate point. The monthly averaged wind speeds were calculated using the mesoscale data and the lidar data. Figs. 3 (a) and (b) show the linear regression analysis for the monthly lidar wind speeds at 100 m height and monthly mesoscale data at 100 m height at coordinates nos. 1 and 3, respectively. The linear line slopes were 0.965 and 1.198 with the R^2 values of 0.862 and 0.936, respectively.

The monthly averaged wind speeds calculated from the lidar and the mesoscale data at the same heights from 50 m to 200 m were compared to obtain the correlation coefficient, as shown in Table 3. The correlation coefficient values between the two sorts of data were comparatively high, ranging from 0.898 to 0.990. The lowest correlation coefficient value appeared at 50 m height at coordinate no. 4, while the highest value was found at 200 m height at the same coordinate point. As the height increased, the average correlation coefficient value increased. The average values along with height were in the range from 0.934 to 0.981, indicating a high correlation between the two kinds of wind data.

Coordinate no.1 had the lowest average correlation coefficient value, with 0.952, while the highest average value of 0.968 was observed at coordinate no. 3. Therefore, the lidar wind data accuracy was high enough to proceed for further analysis.

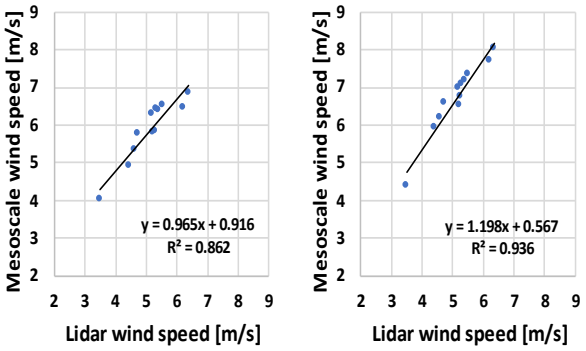

(a) Coordinate no. 1 (b) Coordinate no. 3

Fig. 3 Comparison between mesoscale data and lidar wind speeds at a height of 100 m.

Table 3
Correlation coefficient of mesoscale and lidar data

EMD-WRF South Korea		Height				Average
No.	Coordinate	50 m	100 m	150 m	200 m	
1	N36.02033 E129.2514	0.945	0.928	0.954	0.982	0.952
2	N36.01988 E129.2848	0.957	0.928	0.947	0.978	0.953
3	N36.01943 E129.3181	0.940	0.968	0.976	0.987	0.968
4	N35.99334 E129.2509	0.898	0.966	0.975	0.990	0.957
5	N35.99291 E129.2842	0.950	0.965	0.965	0.975	0.964
6	N35.99244 E129.3176	0.912	0.967	0.970	0.976	0.956
Average		0.934	0.954	0.965	0.981	-

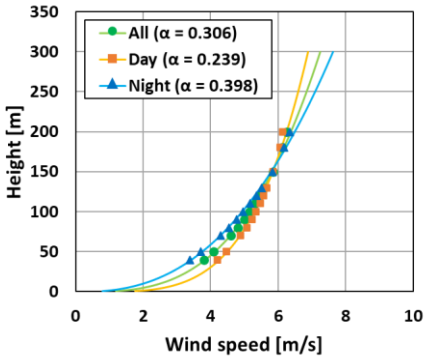

Fig. 4 Vertical profile of lidar wind speeds.

3.2 Wind condition

Fig. 4 shows the vertical profile of lidar wind speeds. The annual average wind speeds at heights from 40 m to 200 m, using all available data, ranged from 3.8 m/s to 6.3 m/s. The wind speeds ranged between 4.2 m/s and 6.1 m/s during the daytime, while ranging from 3.4 m/s to 6.4 m/s during the nighttime at all heights. The difference in the shape of the vertical profile of the daytime and the nighttime was due to atmospheric stability conditions. During the nighttime, the profile can be gentle with mostly stable atmospheric conditions, while during the daytime, it can be steep with prevailing unstable conditions. The average WSE of all data was 0.306, while values during daytime and nighttime were 0.239 and 0.398, respectively. These WSE values indicated the presence of forested areas surrounding the lidar (Aghbalou *et al.,* 2018).

Fig. 5 presents the wind roses at measurement heights of 40 m, 70 m, 100 m and 200 m. At the 40 m height, the prevailing wind direction was from the west, gradually shifting to the west-northwest as the height increased from 70 m to 200 m. The directional distribution also shifted in a clockwise direction as the height increased from 40 m to 200 m, indicating the occurrence of wind veering between the four measurement heights. However, it was found that northerly and southerly winds were much less common. An increase of wind speed was also observed as height increased, with variations in wind speeds from 40 m to 200 m heights.

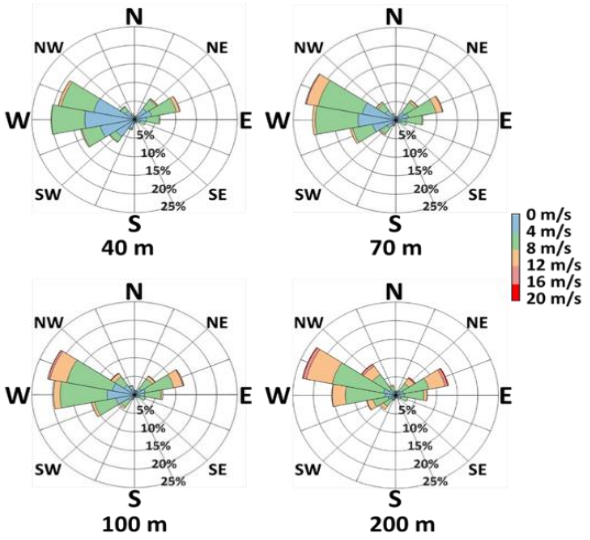

Fig. 5 Wind roses.

3.3 Wind veer characteristics

Figs. 6 (a), (b), (c) and (d) show the distribution of wind direction shifting degrees between 50 m and 40 m heights, 70 m and 50 m heights, 100 m and 90 m heights, and 200 m and 180 m heights. Between 50 m and 40 m heights, wind veer angles were mostly gathered in the range between -1.25 deg./m to 2.25 deg./m, while those between 70 m and 50 m heights were mostly positioned between -1.25 deg./m to 1.25 deg./m. However, between 100 m and 90 m heights and between 200 m and 180 m heights, 81.5 % and 86.0 % of all the wind veer angles were concentrated around zero deg./m, respectively. The wind veer angle distribution was the widest between 50 m and 40 m heights, gradually narrowing with increasing heights. The narrowest distribution of wind veer appeared between 200 m and 180 m heights. This suggests that wind veering occurred more significantly at lower measurement heights due to flow distortion caused by topographical complexity.

The vertical profile of wind veer according to different wind speed ranges is shown in Fig.7 (a). The wind veer value and fluctuation were the largest within the wind speed ranges of 0 m/s to 4 m/s. In general, larger wind veer values and fluctuations were found at the lower wind speed ranges. That is, as the wind speed decreased, the wind veer angle became more significant. The same trend of decreasing wind veer angles with an increase in wind speed were observed by Murphy *et al.* (Murphy *et al.*, 2020) and Tumenbayar et al. (Tumenbayar & Ko, 2023). Since the cut-in wind speed of a wind turbine is typically 3 m/s to 4 m/s, wind speeds lower than 4 m/s were discarded. After discarding the data, the remaining wind data of 37.1 % was used for the following analyses.

Fig. 7 (b) presents the wind veer profile with seasons. The largest wind veer values were observed during the winter season, while the autumn season exhibited the lowest wind veer angles. In the spring season, wind veer values were higher than in the summer season at heights below 100 m, whereas at heights above 100 m, wind veer values were higher during the summer season compared to the spring season. These seasonal trends align with the work of Shu et al. (Shu, Li, He, *et al.,* 2020).

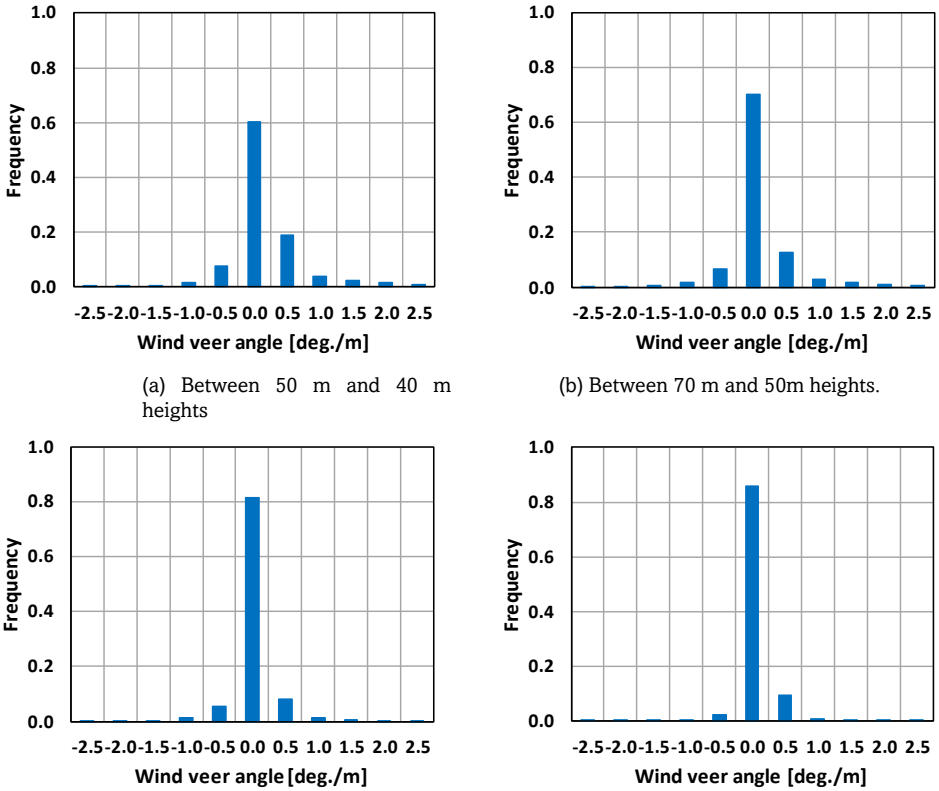

(a) Between 50 m and 40 m heights

(b) Between 70 m and 50m heights.

(c) Between 100 m and 90 m heights.

(d) Between 200 m and 180 m heights.

Fig. 6 Wind direction shifting degrees between two measurement heights.

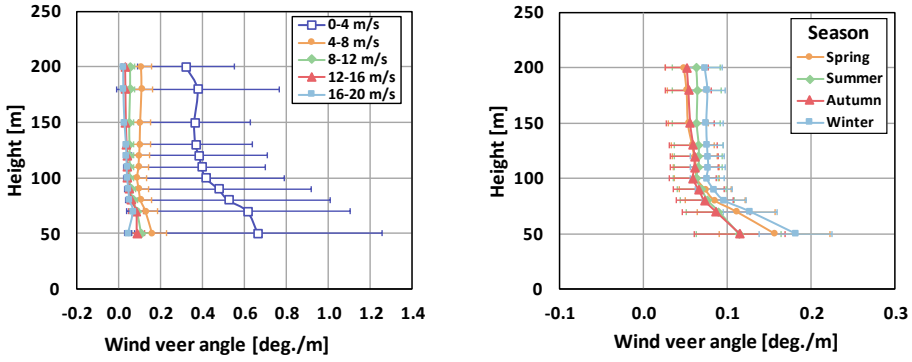

(a) Wind veer with wind speed (b) Wind veer with season

Fig. 7 Vertical profile of wind veer. The error bar corresponds to one standard deviation.

Figs. 8 (a) and (b) represents the diurnal and monthly variations of the wind veer at all measurement heights. In Fig. 8 (a), larger wind veer angles were found during nighttime when the atmosphere was mostly under stable condition compared to daytime when the atmosphere was predominantly unstable (Tumenbayar & Ko, 2023) at all heights. The lower measurement heights had larger wind veer values, which meant that wind veering was more influenced by topographical conditions at lower measurement heights. These results are similar to the findings of Wharton *et al.* (Wharton *et al.*, 2015).

In Fig, 8 (b), the months from June to September had the lowest wind veer values when the unstable atmosphere was prevailing, while the highest values were measured from November to February when the atmosphere was mainly under stable condition (Kikuchi *et al.*, 2020) at heights below approximately 100 m. On the other hand, wind veers at higher measurement heights had a roughly uniform trend across all months. Similar to the diurnal variation, lower measurement heights had higher wind veer values due to topographical effects.

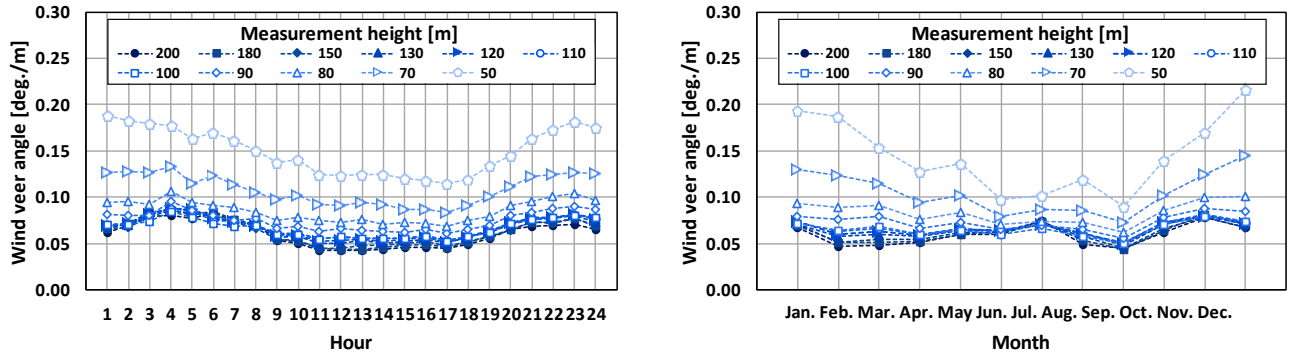

(a) Diurnal variation (b) Monthly variation

Fig. 8 The variation of wind veer value with measurement height..

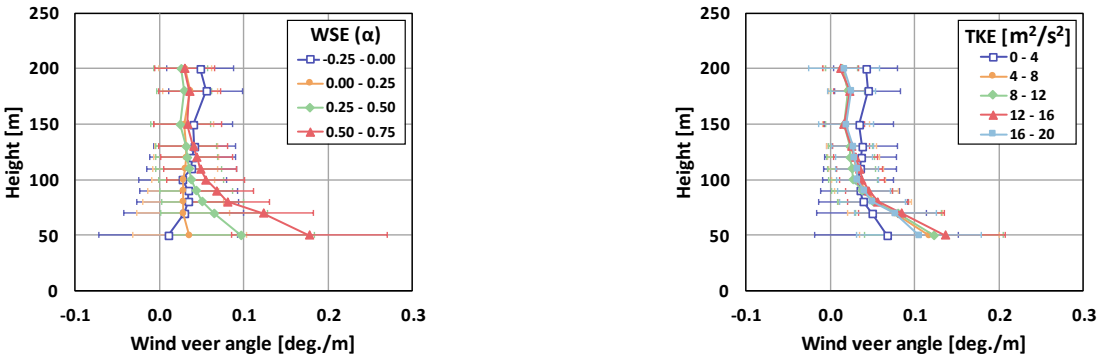

(a) Wind veer with WSE (b) Wind veer with TKE

Fig. 9 Wind veer profile with WSE and TKE. The error bar corresponds to one standard deviation.

Table 4
Relative error of REWS and HHWS by each wind speed bin.

Wind speed bin [m/s]	REWS [%]	HHWS [%]
4	0.05	0.15
5	0.03	0.03
6	0.01	0.05
7	0.01	0.06
8	0.00	0.10
9	0.03	0.10
10	0.02	0.13
11	0.02	0.12
12	0.01	0.13
13	0.00	0.20
14	0.03	0.00
15	0.04	0.44
16	0.22	0.21
17	0.19	0.24
18	0.02	0.04
19	0.02	0.87
20	0.04	0.48
Average	0.04	0.20

The wind veer profiles with respect to WSE and TKE are displayed in Figs. 9 (a) and (b). Higher wind veer values were observed at higher WSE values, except for WSEs between -0.25 and 0.00. The wind veer values decreased with an increase in measurement height for WSEs ranging from 0.00 to 0.75. However, the opposite trend was observed for WSEs between -0.25 and 0.00, as the wind shear exhibited a reverse shape compared to positive WSE values. The wind veer angle decreased with an increase in measurement height for TKE values ranging from 4 m^2/s^2 to 20 m^2/s^2. TKE values lower than 4 m^2/s^2 exhibited similar wind veer values across all measurement heights. Overall, the wind veer values were found to be insensitive to changes in TKE, except for TKE values smaller than 4 m^2/s^2.

Table 4 represents the relative error of REWS and HHWS using the equation (6). The relative error value was calculated for the wind speeds from 4 m/s to 20 m/s, with a bin of 1 m/s. For the REWS, the relative error values ranged from 0.00 % to 0.22 %. On the other hand, the relative error values of HHWS were in the range between 0.00 % and 0.87 %. Wind speeds higher than 15 m/s had the highest error values because of the limited number of measured data points. The average relative errors were 0.04 % and 0.20 % for the REWS and the HHWS, respectively. In other words, the HHWS had higher relative error values than the REWS. The result meant that, even without mentioning the HHWS, using the REWS for estimating power production could lead to larger wind turbine production error, since power production is proportional to the cube of wind speed.

3.4 Atmospheric stability condition

The vertical profiles of wind veer according to atmospheric stability conditions based on WSE and TKE regimes are presented in Figs. 10 (a) and (b). In Fig. 10 (a), the stable condition exhibited the highest wind veer values with high fluctuations at measurement heights lower than 100 m, which then decreased with an increase in height. The wind veer angle of approximately 0.03 deg./m was observed at all measurement heights under neutral conditions. Conversely, wind veer values increased with height under unstable conditions.

In Fig. 10 (b), the stable condition exhibited the highest wind veer values and fluctuations. Under stable conditions, wind veer values decreased up to a measurement height of 100 m and then became almost consistent at higher measurement heights. Wind veer angles under unstable and neutral conditions were smaller and similar to each other as measurement height increased. Additionally, wind veer values at lower measurement heights exhibited larger fluctuations under all atmospheric stability conditions.

In this study, the stable condition had larger wind veer angles and fluctuations, while the unstable and neutral conditions exhibited smaller angles and fluctuations at measurement heights below 100 m.

4. Conclusions

The wind veer characteristics on complex terrain were analysed considering various factors. Wind conditions were measured at heights ranging from 40 m to 200 m using ground-based lidar. The key findings are as follows: Wind veer angles increased with decreasing wind speed. Larger wind veer angles were observed during nighttime compared to daytime at all heights. Winter season exhibited the largest wind veer values, while autumn season exhibited the lowest wind veer angles. The HHWS showed higher relative error values than the REWS. The average relative error values were 0.04 % and 0.20 % for the REWS and the HHWS, respectively, which can lead to larger turbine production errors. The topographical condition of the measurement site significantly influenced the wind veer angle at heights below 100 m. However, the topographical effect

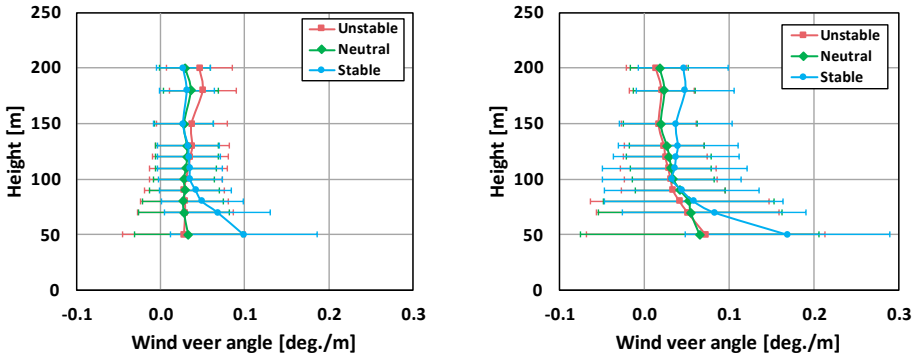

(a) Wind veer with WSE (b) Wind veer with TKE

Fig. 10 Wind veer profile in atmospheric stability conditions. The error bar corresponds to one standard deviation.

gradually decreased at heights above 100 m, which may be a critical height at the studied site.

Acknowledgments

This research was supported by the 2022 Scientific Promotion Program funded by Jeju National University.

Author Contributions: UT.: Conceptualization, Methodology, Software, Formal analysis, Investigation, Writing - original draft, Visualization. KK.: Writing - review & editing, Supervision, Project administration. All authors have read and agreed to the published version of the manuscript.

Conflicts of Interest: The authors declare no conflict of interest.

References

Abkar, M., Sørensen, J. N., & Porté-Agel, F. (2018). An analytical model for the effect of vertical wind veer on wind turbine wakes. *Energies*, *11*(7), 1838. https://doi.org/10.3390/en11071838

Aghbalou, N., Charki, A., Elazzouzi, S. R., & Reklaoui, K. (2018). A probabilistic assessment approach for wind turbine-site matching. *International Journal of Electrical Power & Energy Systems*, *103*, 497–510. https://doi.org/10.1016/j.ijepes.2018.06.018

Bardal, L. M., Sætran, L. R., & Wangsness, E. (2015). Performance test of a 3MW wind turbine–effects of shear and turbulence. *Energy Procedia*, *80*, 83–91. https://doi.org/10.1016/j.egypro.2015.11.410

Barthelmie, R. J., Shepherd, T. J., Aird, J. A., & Pryor, S. C. (2020). Power and Wind Shear Implications of Large Wind Turbine Scenarios in the US Central Plains. *Energies*, 13(16). https://doi.org/10.3390/en13164269

Birkelund, Y., Alessandrini, S., Byrkjedal, Ø., & Monache, L. D. (2018). Wind power predictions in complex terrain using analog ensembles. *J. Phys.: Conf. Ser. 1*102 012008. https://doi.org/10.1088/1742-6596/1102/1/012008

Bodini, N., Lundquist, J. K., & Kirincich, A. (2019). US East Coast lidar measurements show offshore wind turbines will encounter very low atmospheric turbulence. *Geophysical Research Letters*, *46*(10), 5582–5591. https://doi.org/10.1029/2019GL082636

Borraccino, A., Schlipf, D., Haizmann, F., & Wagner, R. (2017). Wind field reconstruction from nacelle-mounted lidar short-range measurements. *Wind Energy Science*, 2(1), 269–283. https://doi.org/10.5194/wes-2-269-2017

Durán, P., Meiβner, C., & Casso, P. (2020). A new meso-microscale coupled modelling framework for wind resource assessment: A validation study. *Renewable Energy*, 160, 538–554. https://doi.org/10.1016/j.renene.2020.06.074

EMD International. (n.d.). *EMD-WRF South Korea MesoScale Data Set*. https://www.emd-international.com/data-services/mesoscale-time-series/pre-run-time-series/emd-wrf-south-korea-mesoscale-data-set/

Englberger, A., & Lundquist, J. K. (2020). How does inflow veer affect the veer of a wind-turbine wake? *Journal of Physics: Conference Series*, *1452*(1), 12068. https://doi.org/10.1088/1742-6596/1452/1/012068

Ennis, B. L., White, J. R., & Paquette, J. A. (2018). Wind turbine blade load characterization under yaw offset at the SWiFT facility. *Journal of Physics: Conference Series*, *1037*(5), 52001. https://doi.org/10.1088/1742-6596/1037/5/052001

Gao, L., Li, B., & Hong, J. (2021). Effect of wind veer on wind turbine power generation. *Physics of Fluids*, *33*(1), 15101. https://doi.org/10.1063/5.0033826

Gottschall, J., Papetta, A., Kassem, H., Meyer, P. J., Schrempf, L., Wetzel, C., & Becker, J. (2021). Advancing wind resource assessment in complex terrain with scanning lidar measurements. *Energies*, *14*(11), 3280. https://doi.org/10.3390/en14113280

Gualtieri, G., & Secci, S. (2011). Wind shear coefficients, roughness length and energy yield over coastal locations in Southern Italy. *Renewable Energy*, *36*(3), 1081–1094. https://doi.org/10.1016/j.renene.2010.09.001

International Electrotechnical Commission. (2017). Wind turbines, Part 12-1: Power performance measurements of electricity producing wind turbines,. In *International Electrotechnical Commission* (2nd ed., Vol. 2017). https://webstore.iec.ch/publication/26603

International Electrotechnical Commission. (2022). Wind energy generation systems Part 12-1: Power performance measurements of electricity producing wind turbines. *International Electrotechnical Commission*, 3. https://www.en-standard.eu/csn-en-iec-61400-12-wind-energy-generation-systems-part-12-power-performance-measurements-of-electricity-producing-wind-turbines-overview/

Jung, C., & Schindler, D. (2021). The role of the power law exponent in wind energy assessment: A global analysis. *International Journal of Energy Research*, *45*(6), 8484–8496. https://doi.org/10.1002/er.6382

Kang, D., Hyeon, J., Yang, K., Huh, J., & Ko, K. (2017). Analysis and Verification of Wind Data from Ground-based LiDAR. *Int. J. Renew. Energy Res*, *7*, 937–945. https://doi.org/10.20508/ijrer.v7i2.6211.g7074

Kikuchi, Y., Fukushima, M., & Ishihara, T. (2020). Assessment of a coastal offshorewind climate by means of mesoscale model simulations considering high-resolution land use and sea surface temperature data sets. *Atmosphere*, *11*(4), 1–16. https://doi.org/10.3390/ATMOS11040379

Kim, D., Kim, T., Oh, G., Huh, J., & Ko, K. (2016). A comparison of ground-based LiDAR and met mast wind measurements for wind resource assessment over various terrain conditions. *Journal of Wind Engineering and Industrial Aerodynamics*, *158*, 109–121. https://doi.org/10.1016/j.jweia.2016.09.011

Leosphere. (2014). *Windcube V2 liDAR Remote Sensor User Manual*.

Lundquist, J. K. (2022). Wind Shear and Wind Veer Effects on Wind Turbines. In *Handbook of Wind Energy Aerodynamics* (pp. 1–22). Springer. https://doi.org/10.1007/978-3-030-05455-7_44-1

Mason, P. J. (1992). Large-eddy simulation of dispersion in convective boundary layers with wind shear. *Atmospheric Environment Part A, General Topics*, *26*(9), 1561–1571. https://doi.org/10.1016/0960-1686(92)90056-Q

Mortensen, N. G., Tindal, A., & Landberg, L. (2008). Field validation of the RIX performance indicator for flow in complex terrain. *2008 European Wind Energy Conference and Exhibition*. https://backend.orbit.dtu.dk/ws/portalfiles/portal/107110613/Field_validation.pdf

Murphy, P., Lundquist, J. K., & Fleming, P. (2020). How wind speed shear and directional veer affect the power production of a megawatt-scale operational wind turbine. *Wind Energy Science*, *5*(3), 1169–1190. https://doi.org/10.5194/wes-5-1169-2020

Nassif, F. B., Pimenta, F. M., Assireu, A. T., D'Aquino, C. de A., & Passos, J. C. (2020). Wind measurements using a LIDAR on a buoy. *RBRH*, *25*. https://doi.org/10.1590/2318-0331.252020200053

Oh, H., & Kim, B. (2015). Comparison and verification of the deviation between guaranteed and measured wind turbine power performance in complex terrain. *Energy*, *85*, 23–29. https://doi.org/10.1016/j.energy.2015.02.115

Radünz, W. C., Sakagami, Y., Haas, R., Petry, A. P., Passos, J. C., Miqueletti, M., & Dias, E. (2020). The variability of wind resources in complex terrain and its relationship with atmospheric stability. *Energy Conversion and Management*, *222*, 113249. https://doi.org/10.1016/j.enconman.2020.113249

Rasaq, A. K., Baba, R. A., Ayomide, G. A., Oladimeji, A. G., & Idris, O. A. (2015). Assessment of wind resource for possibility of small wind turbine installation in Ilorin, Nigeria. *KKU Engineering Journal*, *42*(4), 298–305. https://doi.org/10.14456/kkuenj.2015.35

Rehman, S., & Al-Abbadi, N. M. (2005). Wind shear coefficients and their effect on energy production. *Energy Conversion and Management*, *46*(15–16), 2578–2591. https://doi.org/10.1016/j.enconman.2004.12.005

Robertson, A. N., Shaler, K., Sethuraman, L., & Jonkman, J. (2019). Sensitivity analysis of the effect of wind characteristics and turbine properties on wind turbine loads. *Wind Energy Science*, *4*(3), 479–513. https://doi.org/10.5194/wes-4-479-2019

Sanchez Gomez, M., & Lundquist, J. K. (2020a). The effect of wind direction shear on turbine performance in a wind farm in central Iowa. *Wind Energy Science*, *5*(1), 125–139. https://doi.org/10.5194/wes-5-125-2020

Sanchez Gomez, M., & Lundquist, J. K. (2020b). The Effects of Wind Veer During the Morning and Evening Transitions. *Journal of*

Physics: Conference Series, *1452*(1), 12075. https://doi.org/10.1088/1742-6596/1452/1/012075

Sharma, P. K., Gautam, A., Baredar, P., Warudkar, V., Bhagoria, J. L., & Ahmed, S. (2021). Analysis of terrain of site Mamatkheda Ratlam through wind modeling tool ArcGIS and WAsP. *Materials Today: Proceedings*, *46*, 5661–5665. https://doi.org/10.1016/j.matpr.2020.09.638

Shaw, W. J., Berg, L. K., Debnath, M., Deskos, G., Draxl, C., Ghate, V. P., Hasager, C. B., Kotamarthi, R., Mirocha, J. D., & Muradyan, P. (2022). Scientific challenges to characterizing the wind resource in the marine atmospheric boundary layer. *Wind Energy Science*, *7*(6), 2307–2334. https://doi.org/10.5194/wes-7-2307-2022

Shin, D., Ko, K., Kang, M. M., Ryu, D., Kang, M. M., & Kim, H. (2019). Comparison of wind turbine power curves using cup anemometer and pulsed doppler light detection and ranging systems. *Journal of Mechanical Science and Technology*, *33*(4), 1663–1671. https://doi.org/10.1007/s12206-019-0318-x

Shu, Z., Li, Q., He, Y., & Chan, P. W. (2020). Investigation of marine wind veer characteristics using wind lidar measurements. *Atmosphere*, *11*(11), 1178. https://doi.org/10.3390/atmos11111178

Shu, Z., Li, Q. S., Chan, P. W., & He, Y. C. (2020). Seasonal and diurnal variation of marine wind characteristics based on lidar measurements. *Meteorological Applications*, *27*(3), e1918. https://doi.org/10.1002/met.1918

Sletsjøe, H. (2020). *Complex terrain: from ruggedness index (RIX), towards physical parameterization*. Delft University of Technology.

St Martin, C. M., Lundquist, J. K., Clifton, A., Poulos, G. S., & Schreck, S. J. (2016). Wind turbine power production and annual energy production depend on atmospheric stability and turbulence. *Wind Energy Science*, *1*(2), 221–236. https://doi.org/10.5194/wes-1-221-2016

Tumenbayar, U., & Ko, K. (2023). An Effect of Wind Veer on Wind Turbine Performance. *International Journal of Renewable Energy Development*, *12*(1). https://doi.org/10.14710/ijred.2023.47905

Wagner, R., Antoniou, I., Pedersen, S. M., Courtney, M. S., & Jørgensen, H. E. (2009). The influence of the wind speed profile on wind turbine performance measurements. *Wind Energy*, *12*(4), 348–362. https://doi.org/10.1002/we.297

Wagner, R., Courtney, M., Gottschall, J., & Lindelöw-Marsden, P. (2011). Accounting for the speed shear in wind turbine power performance measurement. *Wind Energy*, *14*(8), 993–1004. https://doi.org/10.1002/we.509

Wharton, S., Newman, J. F., Qualley, G., & Miller, W. O. (2015). Measuring turbine inflow with vertically-profiling lidar in complex terrain. *Journal of Wind Engineering and Industrial Aerodynamics*, *142*, 217–231. https://doi.org/10.1016/j.jweia.2015.03.023

Yan, B. W., Li, Q. S., Chan, P. W., He, Y. C., & Shu, Z. R. (2022). Characterising wind shear exponents in the offshore area using Lidar measurements. *Applied Ocean Research*, *127*, 103293. https://doi.org/10.1016/j.apor.2022.103293